Eur. J. Mineral.
2013, **25**, 1005–1016

Lead-antimony sulfosalts from Tuscany (Italy). XIV. Disulfodadsonite, $Pb_{11}Sb_{13}S_{30}(S_2)_{0.5}$, a new mineral from the Ceragiola marble quarry, Apuan Alps: occurrence and crystal structure

Paolo ORLANDI[1], Cristian BIAGIONI[1,*], Yves MOËLO[2] and Elena BONACCORSI[1]

[1] Dipartimento di Scienze della Terra, Università di Pisa, Via S. Maria 53, 56126 Pisa, Italy
*Corresponding author, e-mail: biagioni@dst.unipi.it
[2] Institut des Matériaux Jean Rouxel, UMR 6502, CNRS, Université de Nantes, 2 rue de la Houssinière, 44322 Nantes Cedex 3, France

Abstract: The new mineral species disulfodadsonite, $Pb_{11}Sb_{13}S_{30}(S_2)_{0.5}$, has been discovered in a cavity of the Liassic marbles quarried in the Ceragiola area, near the town of Seravezza, Apuan Alps, Tuscany, Italy. It occurs as acicular crystals, up to 3–4 mm in length and a few micrometers in width, associated with boulangerite, calcite, and sphalerite. Disulfodadsonite is metallic black. Under the ore microscope, it is white with red internal reflections visible on the grain edges; no pleochroism could be distinguished. Anisotropy is weak but distinct, with rotation tints from brown to dark blue. Electron microprobe analyses collected on two different grains give (wt %): Pb 46.42(20), Sb 32.29(32), As 0.41(2), S 20.19(13), Cl 0.03(2), total 99.34(58), and Pb 46.76(55), Sb 32.30(32), As 0.40(4), S 20.64(9), Cl 0.02(1), total 100.12(35). On the basis of $\Sigma Me = 48$ apfu, the structural formulae are respectively $Pb_{21.74(8)}(Sb_{25.73(8)}As_{0.53(2)})_{\Sigma=26.26}S_{61.11(24)}Cl_{0.08(4)}$ and $Pb_{21.83(25)}(Sb_{25.66(25)}As_{0.51(4)})_{\Sigma=26.17}S_{62.27(41)}Cl_{0.06(2)}$, close to $Pb_{22}Sb_{26}S_{62}$ (against $Pb_{23}Sb_{25}S_{60}Cl$ for dadsonite). The crystal structure study gives a triclinic unit cell, space group *P*-1, with *a* 4.1192(3), *b* 17.4167(14), *c* 19.1664(16) Å, α 96.127(6), β 90.015(7), γ 91.229(7)°, *V* 1366.9(2) Å^3. Main diffraction lines of the powder diagram, corresponding to multiple *hkl* indices, are (relative visual intensity): 3.820 (ms), 3.649 (s), 3.416 (s), 3.381 (vs), 2.857 (ms), 1.897 (ms). The mean crystal structure of disulfodadsonite has been solved by X-ray single-crystal study on the basis of 3389 reflections with a final $R_1 = 0.102$. It agrees with the general features of dadsonite but without any visible superstructure. The unit-cell content is $Pb_{11}Sb_{13}S_{30}(S_2)_{0.5}$ ($Z = 1$). There are five pure Pb and five pure Sb sites, two mixed (Sb/Pb) sites, and sixteen S positions. The structure can be described as formed by rod-layers, with two types of rod-layers alternating along the **b** stacking direction. Disulfodadsonite is the Cl-free homeotype of dadsonite, $Pb_{23}Sb_{25}S_{60}Cl$, stabilized by the disulfide ion $(S_2)^{2-}$, and related by the coupled substitution $Pb^{2+} + Cl^- \rightarrow Sb^{3+} + (S_2)^{2-}$. Its formation is dependent upon a high value of $f(S_2)$, like other associated minerals at Seravezza (native sulfur, enargite, moëloite, *etc*).

Key-words: disulfodadsonite, new mineral species, sulfosalt, lead, antimony, crystal structure, Seravezza, Apuan Alps, Tuscany, Italy.

1. Introduction

The Apuan Alps are known world-wide for their marble quarries, particularly the famous quarries near the town of Carrara. Marble from Apuan Alps has been quarried for more than twenty centuries and has been appreciated since the Roman times. In the cavities of the Carrara marbles, over one hundred mineral species have been identified (Orlandi, 2007; Orlandi & Criscuolo, 2009), and this is the type-locality for three of them: carraraite, zaccagnaite, and zincalstibite (Merlino & Orlandi, 2001; Bonaccorsi *et al*., 2007).

Other smaller quarrying districts are located in the Apuan Alps; for the study of Pb/(Sb,As) acicular sulfosalts, the most important of these districts is that of Seravezza, located about 20 km southwest of Carrara. The marble quarries are on the eastern slope of the Monte Trambiserra (Pitone area) and on the southwestern slopes of Monte Ornato (Ceragiola and Monte Costa areas). A description of the mineral species found in this locality is reported by Orlandi *et al*. (1996). This area is the type locality for the lead-antimony sulfosalt moëloite (Orlandi *et al*., 2002) and a series of other rare sulfosalts has been described from these quarries: guettardite (Bracci *et al*., 1980), robinsonite (Franzini *et al*., 1992), Sb-rich baumhauerite (Orlandi *et al*., 1996), sartorite (Orlandi & Criscuolo, 2009), and izoklakeite (Orlandi *et al*., 2010), together with the more common species boulangerite and zinkenite.

Orlandi (2007) also cited the occurrence of dadsonite in the cavities of the Seravezza marbles on the basis of X-ray

0935-1221/13/0025-2330 $ 5.40
DOI: 10.1127/0935-1221/2013/0025-2330

powder diffraction patterns. However, chemical analyses pointed out that this specimen is quite completely devoid of chlorine, which permitted to define it as a new mineral species, disulfodadsonite. The mineral and its name have been approved by the CNMNC-IMA, under number 2011–076. The holotype specimen of disulfodadsonite is deposited in the mineralogical collection of the Museo di Storia Naturale, Università di Pisa, Via Roma 79, Calci, Pisa, Italy, with catalogue number 19442. The name emphasizes the homeotypic relationship between disulfodadsonite and dadsonite, with the former stabilized by the disulfide ion $(S_2)^{2-}$.

The aim of this paper is the description of this new lead-antimony sulfosalt from the marble quarries of the Ceragiola area, near Seravezza.

2. Geological setting

The Apuan Alps are a tectonic window that exposes the deepest portion of the Northern Apennines, represented by metamorphic units belonging to the Apuan Alps metamorphic complex. The latter is formed by the Apuane Unit, the Massa Unit, and the Fornovolasco-Panie Unit. These rocks are metamorphosed up to the greenschist facies (Franceschelli *et al.*, 1997; Jolivet *et al.*, 1998; Franceschelli & Memmi, 1999; Molli *et al.*, 2000) and are affected by two main deformation events: a first compressional D_1 phase, dated to 27 Ma, and an extensional D_2 phase, dated to 12–8 Ma (Kligfield *et al.*, 1986; Carmignani & Kligfield, 1990).

The Seravezza marbles, Liassic in age, crop out at the southwestern rim of the tectonic window of Apuan Alps; they are located near the boundary between the Massa Unit and the phyllitic Paleozoic basement of the Apuane Unit. At Seravezza, minerals occur in cavities formed by the deformation processes during the Tertiary Alpine orogeny. Cavities have an elongated, sometimes s-shaped cross-section, only a few millimeters to few centimeters wide and 10 to 30 cm high; the length can reach several meters. These cavities lie *en échelon* on definite horizons related to the schistosity surface of the D_1 tectonic phase, which was refolded during D_2 (Orlandi *et al.*, 1996).

3. Occurrence and mineral description

Disulfodadsonite was identified in a specimen collected at the Ceragiola marble quarries; it occurs in a cm-sized cavity, associated with boulangerite, calcite, and yellow sphalerite, forming very thin black acicular [100] crystals, up to 3–4 mm in length and a few micrometers in width. The streak is black and the luster metallic.

The optical properties are probably very close to those of dadsonite, but the low amount of available material as well as the poor quality of the two studied grains (samples # 4819 and # 4817) in polished section allowed only basic qualitative observations under the microscope. In sample # 4819, the mineral is white, and no pleochroism could be discerned. With crossed polars, anisotropy is weak but distinct, from brown to dark blue. Minute red internal reflections are visible at grain edges. Polysynthetic twinning, characteristic of dadsonite and also suggested by the structural study of disulfodadsonite (see below), may be present but, to be observed, it would need a better quality of surface polish than was obtained here.

The mineral is brittle; the hardness and the density could not be measured due to the small size of the studied material. On the basis of the chemical composition, the calculated density for the two studied samples was 5.854 and 5.881 g/cm^3 for samples # 4819 and # 4817, respectively. The density corresponding to the ideal formula $Pb_{11}Sb_{13}S_{30}(S_2)_{0.5}$ is 5.898 g/cm^3.

3.1. Chemical analysis

Two fragments of disulfodadsonite (samples # 4819 and # 4817) were analyzed with a CAMEBAX SX50 electron microprobe (BRGM-CNRS-University common laboratory, Orléans, France). The operating conditions were: accelerating voltage 20 kV, beam current 20 nA, beam size 1 μm; standards (element, emission line, counting times for one spot analysis) are: pyrite (S $K\alpha$, 20 s), vanadinite (Cl $K\alpha$, 60 s), stibnite (Sb $L\alpha$, 20 s), GaAs (As $L\alpha$, 30 s), and galena (Pb $M\alpha$, 20 s). Two samples of dadsonite from France (Saint-Pons and Le Hangard) were analyzed at the same time and used as internal standards for Cl (0.34 and 0.28 wt % Cl, respectively – Moëlo, 1983) in order to verify the negligible Cl content of disulfodadsonite.

The chemical analyses of the two different fragments of disulfodadsonite analyzed are given in Table 1. In order to compare its chemical formula with that of dadsonite, ideally $Pb_{23}Sb_{25}S_{60}Cl$, the formula of disulfodadsonite was calculated on the basis of $\Sigma Me = 48$ atoms per formula unit (apfu). Sample # 4819 corresponds to $Pb_{21.74(8)}(Sb_{25.73(8)}As_{0.53(2)})_{\Sigma=26.26}S_{61.11(24)}Cl_{0.08(4)}$, whereas sample # 4817 has empirical chemical formula $Pb_{21.83(25)}(Sb_{25.66(25)}As_{0.51(4)})_{\Sigma=26.17}S_{62.27(41)}Cl_{0.06(2)}$. These two formulae are close to the stoichiometry $Pb_{22}Sb_{26}S_{62}$ (*i.e.* 2 × $Pb_{11}Sb_{13}S_{31}$), derived from that of dadsonite by the substitution $Pb^{2+} + Cl^- \rightarrow Sb^{3+} + (S_2)^{2-}$. However, consideration of the formal charges shows that if it is correct, then this formula is not charge-balanced.

Comparison of the analyses of dadsonite and disulfodadsonite given in Table 1 confirms that the latter is systematically richer in S, and that this causes an apparent charge balance problem. The ''Valence Equilibrium'', Ev, is defined as $100 \times [\Sigma(\text{val}+) - \Sigma(\text{val}-)]/\Sigma(\text{val}-)$ where ''val + '' is cation formal valence, and ''val–'' is that of anions (Moëlo *et al.*, 1984). Ev is nil or negative for disulfodadsonite, while it is positive for dadsonite. In particular, the compositions of samples # 4817 of disulfodadsonite and dadsonite from Saint-Pons perfectly agree with their respective ideal compositions, taking into account error margins. Nevertheless, without dadsonite as an

Table 1. Electron-microprobe analyses of disulfodadsonite and dadsonite: chemical composition as wt % (upper part) and number of atoms on the basis of $\Sigma Me = 48$ *apfu*.

	Disulfodadsonite			Dadsonite		
Element	#4819	#4817	Theor.*	Saint-Pons	Le Hangard	Theor.
	wt.%	wt.%	wt.%	wt.%	wt.%	wt.%
Pb	46.42(20)	46.76(55)	46.94	48.54(40)	48.16(21)	48.78
Sb	32.29(32)	32.30(32)	32.59	31.45(13)	31.91(24)	31.16
As	0.41(2)	0.40(4)	–	n.d.	n.d.	–
S	20.19(13)	20.64(9)	20.47	19.60(13)	19.64(5)	19.70
Cl	0.03(2)	0.02(1)	–	0.32(2)	0.28(1)	0.36
Total	99.34(58)	100.12(35)	100	99.91(31)	99.99(31)	100
	apfu	apfu	apfu	apfu	apfu	apfu
Pb	21.74(8)	21.83(25)	22	22.83(13)	22.56(12)	23
Sb	25.73(8)	25.66(25)	26	25.17(13)	25.44(12)	25
As	0.53(2)	0.51(4)	–	0	0	–
S	61.11(24)	62.27(41)	62	59.58(52)	59.44(15)	60
Cl	0.08(4)	0.06(2)	–	0.87(5)	0.76(2)	1
Ev**	0.0(5)	−2.0(8)	−1.6	1.0(8)	1.5(3)	0
Pb/(Sb + As)$_{at.}$	0.828	0.834	0.846	0.907	0.887	0.92

* $Pb_{11}Sb_{13}S_{31}$. ** Relative error on the valence equilibrium (%), calculated as 100 × [Σ(val +) – Σ(val –)]/Σ(val –).

internal standard, such an S excess is difficult to prove; together with the Cl content, the most significant chemical difference is the Pb/(Sb + As) atomic ratio, below 0.85 for disulfodadsonite, and over 0.88 for dadsonite.

3.2. Crystallography

The X-ray powder diffraction pattern of disulfodadsonite was obtained using a 114.6 mm diameter Gandolfi camera, with Ni-filtered Cu *Kα* radiation. The observed X-ray powder pattern is compared with the calculated one (obtained using the software Powdercell; Kraus & Nolze, 1996) in Table 2. Unit-cell parameters were not refined from the X-ray powder diffraction data because of the multiplicity of indices for the majority of diffraction lines. It is important to stress that the diffraction pattern is very similar to that of dadsonite and a distinction between these two phases based upon X-ray powder diffraction techniques appears very problematic (Fig. 1).

For the resolution of the crystal structure, several needle-like crystals were investigated with a Bruker Smart Breeze diffractometer equipped with an air-cooled CCD detector using graphite-monochromated Mo *Kα* radiation. Finally, a crystal suitable for structural investigation was found. Three datasets of 963 frames were collected in 0.5° slices with an exposure time of 45 s. The detector-to-crystal working distance was set to 50 mm. Data were integrated and corrected for Lorentz and polarization, background effects, and absorption using Apex 2 (Bruker AXS Inc., 2004), resulting in 5611 unique reflections. The structure was solved by direct methods using Shelxs-97 and refined using Shelx-97 (Sheldrick, 2008) in a triclinic setting, with unit-cell parameters *a* 4.1192(3), *b* 17.4167(14), *c* 19.1664(16) Å, *α* 96.127(6), *β* 90.015(7), *γ* 91.229(7)°, *V* 1366.9(2) Å^3. The ratio *a*:*b*:*c* is 0.2365:1:1.1005. Scattering curves for neutral atoms were taken from the International Tables for X-ray Crystallography (Wilson, 1992). Initially the crystal structure was solved in the space group *P*1, as suggested by the statistical tests on the distribution of |*E*| values ($|E^2\text{-}1| = 0.782$). The solution was successful and the crystal structure was refined down to $R_1 = 10.1$ %, showing features similar to those displayed by the 4 Å structure of dadsonite (Makovicky *et al.*, 2006). However, the anisotropic displacement parameters of most of the cation sites were negatively defined and, in addition, the racemic twin ratio pointed to an approximately equal amount of the two components, suggesting a higher symmetry, *i.e.* *P*-1. A new refinement was consequently started, using the atomic coordinates given by Makovicky *et al.* (2006) for the average structure of dadsonite. The isotropic refinement converged to $R_1 = 13.2$ %. At this stage of the refinement, the equivalent displacement parameter of Sb1 was too low in comparison with those of the other Sb sites; for this reason, some lead was introduced in Sb1 and the site occupancy was refined. The pair Sb2/Pb6 described by Makovicky *et al.* (2006) in the crystal structure of dadsonite does not occur in disulfodadsonite; on the contrary, a pair Sb2a/Sb2b is present. The occupancies of the other cation sites were initially refined using the following scattering curves: Pb *vs* □ for Pb sites and Sb *vs* □ for Sb sites. All the sites but the Sb4 one are pure Pb or Sb sites and their occupancy was fixed; Sb4 showed a small excess of electron density, compatible with a minor substitution of Sb by Pb. Consequently, its site occupancy was refined using the curves Sb *vs* Pb.

Introducing anisotropic displacement parameters, S and S9 sites displayed too large values, indicating a possible splitting. A new S site was located at a general position (*x*,*y*,*z*), with site occupancy 0.5; S9 site was split into two sub-positions, *i.e.* S9a and S9b. The short S–S distance of ~ 2.3 Å between S and S9b agrees with the occurrence of S–S bonds in disulfodadsonite. During the refinement the occurrence of twinning was accounted for assuming a

Table 2. Observed and calculated X-ray powder diffraction data for disulfodadsonite.

I_{obs}	d_{meas}	I_{calc}	d_{calc}	*h k l*	I_{obs}	d_{meas}	I_{calc}	d_{calc}	*h k l*
vw	9.8	2	9.53	0 0 2	**ms**	**2.814**	27	2.801	−1 0 5
w	8.3	24	8.22	0–2 1			19	2.799	1–1 5
vw	7.55	11	7.58	0 2 1			37	2.794	1 0 5
w	5.73	9	5.69	0–3 1			23	2.793	−1–1 5
w	4.34	11	4.32	0–4 1	m	2.74	12	2.757	−1–4 3
m	4.125	20	4.118	1 0 0			12	2.740	0–6 3
		38	4.109	0–4 2			30	2.734	1–2 5
		25	4.061	0 3 3			38	2.716	−1–2 5
		20	3.997	0 2 4	mw	2.676	24	2.669	0 5 4
		12	3.882	1 1 1	w	2.65	21	2.636	1–4 4
ms	**3.82**	50	3.811	0 0 5	w	2.531	8	2.528	0 6 3
		21	3.809	0–1 5	w	2.483	8	2.467	−1 1 6
		24	3.750	1–2 0	w	2.375	11	2.365	1–6 2
		40	3.688	1 2 0	w	2.355	17	2.347	−1–6 1
s	**3.649**	29	3.653	−1–2 1	mw	2.269	11	2.261	0–5 7
		27	3.643	1 1 2	m	2.243	13	2.248	−1–4 6
		58	3.636	0–2 5			22	2.236	0 2 8
		23	3.589	1 2 1			17	2.227	1 6 2
vw	3.457	13	3.439	−1 2 2			16	2.220	1 1 7
s	**3.416**	95	3.411	0 4 3	w	2.192	10	2.174	−1 6 3
vs	**3.381**	100	3.372	0–5 2	w	2.131	13	2.135	1 6 3
		11	3.300	−131	mw	2.076	15	2.068	0–5 8
		17	3.254	1–3 2			34	2.059	2 0 0
mw	3.188	15	3.176	0 0 6	mw	2.009	14	2.008	0 2 9
		14	3.169	−1 2 3	vw	1.980	10	1.999	0 4 8
		25	3.132	−1 3 2			9	1.972	−1 2 8
mw	3.106	14	3.125	1 2 3	m	1.945	6	1.942	1–8 1
		13	3.112	1 0 4			7	1.936	0–7 7
		10	3.090	0–2 6			9	1.933	1–8 0
		19	3.067	1–3 3	**ms**	**1.897**	15	1.895	−1 3 8
mw	3.044	10	3.046	0 4 4			21	1.894	0 9 1
		17	3.021	1–3 3			12	1.878	1–6 7
mw	3.013	14	3.014	1–4 1	m	1.865	14	1.857	−1–6 7
		38	2.986	−1–2 4	w	1.824	7	1.824	2 3 3
mw	2.922	17	2.912	0 5 3			10	1.814	−2 0 5
		38	2.886	−1 2 4	mw	1.797	12	1.797	2–2 5
ms	**2.857**	24	2.851	1 2 4			11	1.777	−2 4 3
		41	2.847	0–6 2	m	1.736	12	1.727	−1–2 10
		32	2.843	1–3 4	mw	1.71	14	1.685	2–6 2

Notes: the d_{hkl} values were calculated on the basis of the unit cell refined by using single-crystal data. Intensities were calculated on the basis of the structural model. Observed intensities were visually estimated. vs = very strong; *s* = strong; ms = medium-strong; *m* = medium; mw = medium-weak; *w* = weak; vw = very weak. Only reflections with $I_{calc} > 10$ are listed, if not observed.

[100] twin axis (twin obliquity 1.26°), significantly improving the final *R* value; the twin ratio is 93:7.

The formula unit is $Pb_{5.38}Sb_{6.62}S_{15.5}$. The total refined site scattering value at the cation sites is 1557.6 electrons per 2 formula units (epfu), to be compared with 1555.7 epfu (sample # 4819) and 1557.2 epfu (sample # 4817) obtained from the chemical data.

The anisotropic refinement of disulfodadsonite yielded a final R_1 = 10.2 % for 3389 observed reflections. Notwithstanding the relatively high *R* value, the structure solution can be considered satisfactory as regards atom coordinations, values of *Me*–S bond distances, and displacement parameters, and allows the description of the main structural features of disulfodadsonite. Table 3 summarizes the crystal data, the parameters of the data collection, and crystal structure refinement.

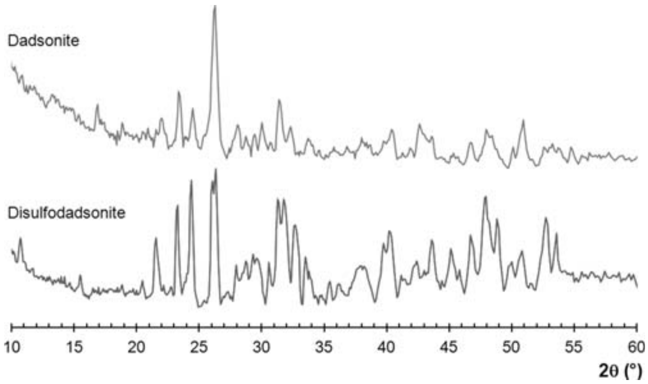

Fig. 1. Comparison between the X-ray powder diffraction patterns of disulfodadsonite and dadsonite from Buca della Vena mine (Orlandi *et al.*, 2010).

Table 3. Crystal data and summary of parameters describing data collection and refinement for disulfodadsonite.

Crystal data	
X-ray formula	$Pb_{5.38}Sb_{6.62}S_{15.5}$
Crystal size (mm^3)	0.18 × 0.01 × 0.01
Cell setting, space group	Triclinic, *P*-1
a, *b*, *c* (Å)	4.1192(3), 17.4167(14), 19.1664(16)
α, β, γ (°)	96.127(6)°, 90.015(7)°, 91.229(7)°
V (Å^3)	1366.9(2)
Z	2
Data collection and refinement	
Radiation, wavelength (Å)	Mo *K*α, 0.71073
Temperature (K)	293
Maximum observed 2θ	55.14
Measured reflections	11390
Unique reflections	5611
Reflections $F_o > 4\sigma(F_o)$	3389
R_{int} after absorption correction	0.1035
$R\sigma$	0.1480
Range of *h*, *k*, *l*	$-5 \le h \le 5$, $-22 \le k \le 22$, $-24 \le l \le 24$
$R\ [F_o > 4\sigma(F_o)]$	0.1022
R (all data)	0.1607
wR (on F_o^2)	0.2496
Goof	1.056
Number of least squares parameters	273
Maximum and minimum residual peaks (*e*/Å^3)	7.58 (at 0.89 Å from Pb3) −4.37 (at 0.87 Å from Pb3)

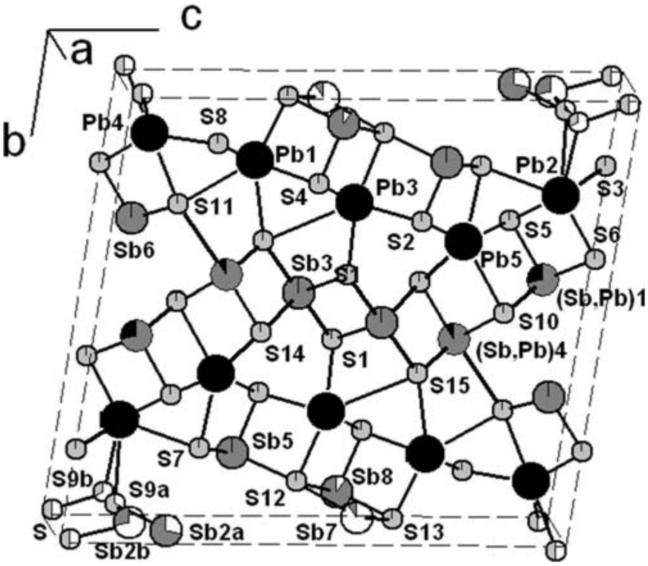

Fig. 2. The unit-cell content of disulfodadsonite. In order of decreasing size, circles represent: lead (black), antimony (gray), and sulphur (light gray).

4. Crystal-structure description

Figure 2 shows the projection along **a** of the crystal structure of disulfodadsonite. Atomic coordinates, equivalent and anisotropic displacement parameters are reported in Tables 4 and 5; selected bond distances are given in Table 6.

4.1. General organization and structure of the rods

The crystal structure of disulfodadsonite agrees with the general features given by Makovicky *et al.* (2006) for dadsonite. It may be described as being formed by lozenge-shaped rods derived from the SnS archetype; as in dadsonite, two kinds of rod-layers alternate along [010], differing in the interconnection of the rods and corresponding to the Type-3 and Type-5 of Makovicky (1993). The rods are three coordination pyramids of Pb and Sb wide, and four combined sulfur-and-metal sheets thick. In every rod, two sulfur-and-metal sheets (A/A' and B/B') are separated by a lone electron pair micelle (Fig. 3).

The Type-3 rod-layer has adjacent rods interconnected by a pair of standing monocapped coordination prisms of Sb, whereas the connection between rods in the Type-5 rod-layer is achieved through a single row of anions. In dadsonite, these anions are represented by chlorine, whereas in disulfodadsonite sulfur replaces the halogen at the S site, forming localized S–S bonds with the split S9b site (Fig. 4), forming an S-rich column. The S–S bond-lengths are generally between ~ 2–2.06 Å, as in livingstonite (Niizeki & Buerger, 1957; Srikrishnan & Nowacki, 1975) and moëloite (Orlandi *et al.*, 2002). The S–S bond distance is ~ 2.15 Å in pyrite (Bayliss, 1977) and ~ 2.2 Å in marcasite (Buerger, 1937). In disulfodadsonite the observed distance, *i.e.* 2.32(6) Å, is a little longer than previously reported S–S distances. However, it is important to bear in mind that all atom positions are mean positions of the substructure, and probably the true structure ought to give shorter distances.

4.2. Cation coordination and site occupancies

The crystal structure of disulfodadsonite shows the presence of five pure Pb sites, five pure Sb sites (among which two are split), two mixed (Sb/Pb) sites, and sixteen S sites (Fig. 2).

The Pb sites are located on the outer surface of the rods. Coordination number ranges between VII and IX. Average bond-lengths range between 3.02 Å for the seven-fold coordinated Pb2 site and 3.13 Å for the nine-fold coordinated Pb4 site; in the average structure of dadsonite the corresponding values range from 3.014 Å for the seven-fold-coordinated Pb2 site to 3.077 Å for the eight-fold-coordinated Pb5 site (Makovicky *et al.*, 2006). The bond-valence sums (BVS; Table 6) of the pure Pb sites are in agreement with the expected values.

Among the Sb sites, two are split. Sb3 connects the rod of Type-3 rod-layers, whereas the remaining Sb sites are located in the inner portion of the rods. In addition to the five pure Sb sites, two sites, namely Sb1 and Sb4, have a mixed (Sb/Pb) site occupancy. Taking into account the Sb–S bond distances shorter than 3.0 Å, all these Sb sites

Table 4. Atomic coordinates and equivalent isotropic displacement parameters (Å^2) for disulfodadsonite. U_{eq} is defined as one third of the trace of the orthogonalized U^{ij} tensor.

Site	Population	*x*	*y*	*z*	U_{eq}
Pb1	$Pb_{1.00}$	0.4694(5)	0.1745(1)	0.2846(1)	0.0199(5)
Pb2	$Pb_{1.00}$	0.4678(5)	0.7563(1)	0.1034(1)	0.0188(5)
Pb3	$Pb_{1.00}$	0.4553(5)	0.2687(1)	0.4962(1)	0.0186(5)
Pb4	$Pb_{1.00}$	0.5001(5)	0.1117(1)	0.0682(1)	0.0261(5)
Pb5	$Pb_{1.00}$	0.4645(5)	0.6517(1)	0.2794(1)	0.0219(5)
Sb1	$Sb_{0.71(2)}Pb_{0.29(2)}$	0.8898(8)	0.5401(2)	0.0921(2)	0.024(1)
Sb2a	$Sb_{0.72(1)}$	0.953(2)	0.9730(3)	0.2101(3)	0.036(1)
Sb2b	$Sb_{0.28(1)}$	0.977(4)	0.9550(8)	0.1352(7)	0.036(1)
Sb3	$Sb_{1.00}$	0.3173(8)	0.4796(2)	0.4208(2)	0.020(1)
Sb4	$Sb_{0.91(3)}Pb_{0.09(3)}$	0.8395(9)	0.4077(2)	0.2505(2)	0.026(1)
Sb5	$Sb_{1.00}$	0.0652(12)	0.8548(2)	0.3558(2)	0.037(1)
Sb6	$Sb_{1.00}$	0.9035(10)	0.6719(2)	0.9211(2)	0.027(1)
Sb7	$Sb_{0.10(3)}$	0.053(23)	0.058(3)	0.418(3)	0.027(2)
Sb8	$Sb_{0.90(3)}$	0.905(3)	0.0610(3)	0.4290(3)	0.027(2)
S	$S_{0.5}$	−0.004(9)	−0.010(2)	0.0191(14)	0.027(6)
S1	$S_{1.00}$	0.965(3)	0.3984(6)	0.4842(6)	0.019(3)
S2	$S_{1.00}$	0.008(3)	0.7249(7)	0.3889(6)	0.016(3)
S3	$S_{1.00}$	0.979(3)	0.7898(7)	0.0024(6)	0.013(2)
S4	$S_{1.00}$	0.972(3)	0.1932(7)	0.3966(6)	0.016(3)
S5	$S_{1.00}$	0.969(3)	0.6665(7)	0.1737(6)	0.013(2)
S6	$S_{1.00}$	0.483(3)	0.6124(7)	0.0160(6)	0.022(3)
S7	$S_{1.00}$	0.504(4)	0.8169(7)	0.2679(6)	0.025(3)
S8	$S_{1.00}$	0.984(3)	0.1043(8)	0.1849(6)	0.020(3)
S9a	$S_{0.67(3)}$	0.500(10)	0.9433(13)	0.1212(12)	0.061(10)
S9b	$S_{0.33(3)}$	0.29(2)	0.931(3)	0.101(3)	0.061(10)
S10	$S_{1.00}$	0.461(3)	0.4919(7)	0.1789(6)	0.021(3)
S11	$S_{1.00}$	0.510(4)	0.2704(7)	0.1464(6)	0.020(3)
S12	$S_{1.00}$	0.516(4)	0.8907(8)	0.4705(7)	0.027(3)
S13	$S_{1.00}$	0.479(3)	0.0278(7)	0.3282(6)	0.018(3)
S14	$S_{1.00}$	0.938(3)	0.5278(6)	0.3323(6)	0.013(2)
S15	$S_{1.00}$	0.415(3)	0.3581(7)	0.3302(6)	0.016(3)

are three- and four-fold coordinated; additional longer bonds increase the coordination number to six. In the S-rich columns (Fig. 4), the coordination of Sb2a is satisfactory, with a slightly short Sb2a–S8 distance of 2.38 Å; however, S8 is a mean position and the real Sb2a–S8 distance could be longer. On the contrary, the coordination of the split position Sb2b is unsatisfactory, with a too short Sb2b–S9a distance of 2.18(5) Å, probably owing to the average position of the S9a site. Like for the S9b site, the S9a site has a high equivalent isotropic displacement parameter, which indicates that S9a is the mean position of (at less) two distinct sub-positions.

Chemical data show the occurrence of about 0.25 As apfu ($Z = 1$). Unfortunately, owing to the quality of the structural refinement, it was not possible to resolve the partitioning of arsenic among Sb positions in the crystal structure of disulfodadsonite.

5. Crystal chemistry

5.1. Structural formula

Through the chemical and structural studies, it appears that disulfodadsonite is the Cl-free homeotype of dadsonite. In fact, it contains only traces of chlorine (0.03 wt % against 0.3–0.4 wt % in dadsonite; Moëlo, 1979) and has a higher S content, coupled with a lower Pb/(Sb + As) atomic ratio. Electrostatic neutrality may be achieved through the heterovalent substitution $Pb^{2+} + Cl^- = Sb^{3+} + (S_2)^{2-}$.

A similar relationship was observed between synthetic $Pb_{6.9}Sb_{5.1}S_{13.1}Cl_{2.9}$ (Doussier *et al.*, 2008) and moëloite, $Pb_6Sb_6S_{14}(S_3)$, where two substitution rules are operating, *i.e.* $2Cl^- = (S_3)^{2-}$ and $Pb^{2+} + Cl^- = Sb^{3+} + S^{2-}$. Moreover, among the lead-antimony chloro-sulfosalts described by Moëlo *et al.* (1989) in the deposit of Les Cougnasses (Hautes-Alpes, France), their ''Mineral C'' is close to the synthetic ''phase V'' of Bortnikov *et al.* (1979) and both phases seem to be related to playfairite through the heterovalent substitution $Sb^{3+} + S^{2-} \rightarrow Pb^{2+} + Cl^{2-}$. Hence, a range of substitution mechanisms occur that involve Pb, Cl, Sb, and S.

The ideal chemical formula of disulfodadsonite may be written as $Pb_{22}Sb_{26}S_{60}(S_2)$. The ideal chemical composition requires (in wt %): Pb 46.94, Sb 32.59, S 20.47. Taking into account the $(S_2)^{2-}$ disulfide anion in order to fit the charge balance, the crystal structure formula must be written, on the basis of 48 cations, as $Pb_{21.52}Sb_{26.48}S_{60.48}(S_2)_{0.76}$. This formula as well as chemical analyses show a $(Pb/Sb)_{at.}$ ratio slightly lower than the ideal one, correlated to a (S_2)

Table 5. Anisotropic displacement parameters for disulfodadsonite.

Site	U^{11}	U^{22}	U^{33}	U^{23}	U^{13}	U^{12}
Pb1	0.020(1)	0.027(1)	0.014(1)	0.004(1)	−0.003(1)	0.002(1)
Pb2	0.020(1)	0.024(1)	0.013(1)	0.005(1)	0.000(1)	0.003(1)
Pb3	0.017(1)	0.024(1)	0.015(1)	0.000(1)	0.000(1)	0.001(1)
Pb4	0.023(1)	0.034(1)	0.022(1)	0.009(1)	−0.003(1)	0.003(1)
Pb5	0.018(1)	0.037(1)	0.012(1)	0.008(1)	0.002(1)	0.007(1)
Sb1	0.028(2)	0.028(2)	0.016(2)	0.011(1)	−0.002(1)	−0.005(1)
Sb2a	0.062(4)	0.019(2)	0.027(3)	0.009(2)	−0.008(3)	0.005(3)
Sb2b	0.062(4)	0.019(2)	0.027(3)	0.009(2)	−0.008(3)	0.005(3)
Sb3	0.017(2)	0.029(2)	0.015(2)	0.010(1)	−0.005(1)	−0.004(1)
Sb4	0.035(2)	0.025(2)	0.018(2)	0.000(1)	0.006(1)	−0.001(2)
Sb5	0.059(3)	0.016(2)	0.039(2)	0.010(2)	0.022(2)	0.011(2)
Sb6	0.044(2)	0.022(2)	0.014(2)	−0.002(1)	−0.014(2)	0.013(2)
Sb7	0.038(6)	0.019(2)	0.027(2)	0.007(2)	−0.001(3)	0.010(2)
Sb8	0.038(6)	0.019(2)	0.027(2)	0.007(2)	−0.001(3)	0.010(2)
S	0.04(2)	0.014(15)	0.03(2)	0.004(11)	−0.017(17)	0.004(12)
S1	0.032(8)	0.011(6)	0.015(6)	0.002(4)	0.015(6)	−0.001(5)
S2	0.019(7)	0.016(6)	0.014(5)	−0.002(4)	0.003(5)	0.006(5)
S3	0.013(6)	0.020(6)	0.007(5)	0.006(4)	−0.003(4)	0.003(5)
S4	0.019(7)	0.017(6)	0.012(5)	0.005(4)	0.003(5)	0.001(5)
S5	0.005(6)	0.026(6)	0.009(5)	0.006(4)	0.004(4)	0.008(5)
S6	0.023(7)	0.019(6)	0.022(6)	−0.003(5)	0.006(6)	−0.002(6)
S7	0.047(9)	0.014(6)	0.014(6)	−0.001(4)	0.008(6)	−0.002(6)
S8	0.011(6)	0.039(8)	0.011(5)	0.015(5)	−0.007(5)	0.001(6)
S9a	0.14(3)	0.014(10)	0.023(12)	0.005(8)	−0.044(14)	−0.009(15)
S9b	0.14(3)	0.014(10)	0.023(12)	0.005(8)	−0.044(14)	−0.009(15)
S10	0.025(7)	0.027(7)	0.009(5)	−0.000(5)	0.001(5)	−0.003(6)
S11	0.039(8)	0.010(6)	0.012(6)	0.003(4)	−0.013(6)	0.003(6)
S12	0.041(9)	0.020(6)	0.020(6)	0.004(5)	0.007(6)	0.002(6)
S13	0.022(7)	0.017(6)	0.014(5)	0.005(4)	−0.009(5)	0.000(5)
S14	0.019(7)	0.014(6)	0.007(5)	0.007(4)	−0.006(5)	−0.000(5)
S15	0.026(7)	0.014(6)	0.008(5)	0.002(4)	0.010(5)	0.000(5)

deficit, which would indicate the substitution $2Pb^{2+} + (S_2)^{2-} \rightarrow 2Sb^{3+} + 2S^{2-}$. Consequently, the general formula of disulfodadsonite may be written as $Pb_{22\text{-}2x}Sb_{26+2x}S_{60+2x}(S_2)_{1\text{-}x}$; the *x* value is 0.24 for the crystal structure, and 0.17 and 0.11 for analyses # 4819 and 4817, respectively.

5.2. S–S bonds in disulfodadsonite and possible ordering in the S-rich column

The connection between Type-5 rod-layers is characterized by the occurrence of unrealistic short distances in the S-rich column between atom pairs with a site-occcupancy factor (s.o.f.) sum equal or close to one [*d*(Å) and s.o.f. sum]: S–S (0.84, 1), S9a–S9b (0.94, 1), Sb2a–Sb2b (1.44, 1), Sb2a–S9a (1.99, 0.95). This clearly indicates an exclusion relationship among these atom pairs, and suggests that each S-rich column has to be ordered along **a**. Nevertheless, superstructure reflections are absent (at least using conventional Mo *K*α radiation and area detector) and consequently it appears difficult to propose a definite ordered model for the connection between Type-5 rods.

The absence of superstructure reflections could be related to the absence of any correlation between one S-rich column and the other columns displaced along **b** and **c**. Some other sulfosalts, *e.g.* jamesonite (Léone *et al.*, 2003) or robinsonite (Franzini *et al.*, 1992; Makovicky *et al.*, 2004), have only the basic 4 Å periodicity, whereas others, like boulangerite and zinkenite may have both the ordered (∼8 Å; Mumme, 1989) and disordered (∼4 Å; Petrova *et al.*, 1978; Skowron & Brown, 1990) variants. Another explanation of the absence of long-range ordering could be the non-stoichiometry of the (S_2) concentration.

6. Discussion

6.1. Comparison between the unit-cell parameters of dadsonite and disulfodadsonite

The unit cell of disulfodadsonite can be compared with the sub-cell of dadsonite (Table 7). The cell volume of disulfodadsonite is ∼ 0.2 % greater than that of dadsonite. A similar relationship was observed between the synthetic $Pb_{6.9}Sb_{5.1}S_{13.1}Cl_{2.9}$ (Doussier *et al.*, 2008) and moëloite, $Pb_6Sb_6S_{14}(S_3)$ (Orlandi *et al.*, 2002). The cell volume of the former is 1420.6 Å^3, whereas the latter has a cell volume of 1427.6 Å^3, corresponding to a $\delta V = +0.5$ %. Although the substitution rules are different, the compounds with S–S pairs show a larger unit-cell volume relative to their Cl-homeotypes.

Table 6. Interatomic bond distances and bond valence sums (BVS), according to Brese & O'Keeffe (1991), around Pb and Sb atoms (in Å).

		d (Å)			*d* (Å)			*d* (Å)			*d* (Å)			*d* (Å)
Pb1	– S13	2.77(1)	Pb2	– S6	2.86(1)	Pb3	– S2	2.91(1)	Pb4	– S11	3.00(1)	Pb5	– S7	2.91(1)
	– S8	2.92(1)		– S3	2.90(1)		– S12	2.92(1)		– S	3.01(3)		– S5	2.91(1)
	– S4	2.96(1)		– S3	2.95(1)		– S4	2.95(1)		– S8	3.01(1)		– S5	2.93(1)
	– S4	2.97(1)		– S5	2.97(1)		– S1	3.08(1)		– S	3.05(4)		– S2	3.02(1)
	– S8	3.04(1)		– S5	3.02(1)		– S4	3.08(1)		– S3	3.05(1)		– S14	3.18(1)
	– S15	3.24(1)		– S9b	3.16(5)		– S1	3.09(1)		– S	3.06(3)		– S10	3.21(1)
	– S11	3.28(1)		– S7	3.22(1)		– S2	3.11(1)		– S8	3.10(1)		– S2	3.22(1)
				– S9a	3.24(2)		– S15	3.69(1)		– S3	3.12(1)		– S14	3.27(1)
	mean	3.03		mean	3.02		mean	3.10		– S	3.13(4)		mean	3.08
	BVS	2.12		BVS	2.02		BVS	2.07		– S9a	3.20(2)		BVS	2.06
		(2.00)			*(2.00)*			*(2.00)*		– S9b	3.36(5)			*(2.00)*
										– S9b	3.37(6)			
										– S9a	3.65(2)			
										mean	3.13			
										BVS	2.02			
											(2.00)			
		d (Å)			*d* (Å)			*d* (Å)			*d* (Å)			*d* (Å)
Sb1	– S5	2.57(1)	Sb2a	– S8	2.39(1)	Sb2b	– S9a	2.18(5)	Sb3	– S1	2.42(1)	Sb4	– S14	2.50(1)
	– S10	2.61(1)		– S9a	2.54(3)		– S	2.37(3)		– S14	2.53(1)		– S15	2.52(1)
	– S6	2.64(1)		– S9b	2.55(7)		– S8	2.67(2)		– S15	2.63(1)		– S10	2.64(1)
	– S10	3.07(1)		– S9a	2.85(4)		– S9b	2.91(9)		– S1	2.91(1)		– S15	3.01(1)
	– S6	3.15(1)		– S13	3.08(1)		– S	3.20(3)		– S14	3.21(1)		– S11	3.22(1)
	– S6	3.52(1)		– S13	3.19(1)		– S3	3.63(2)		– S1	3.33(1)		– S10	3.30(1)
				– S9b	3.46(7)									
	mean^1	2.61		– S7	3.53(1)		mean			mean^1	2.62		mean^1	2.55
	mean^2	2.93		– S	3.71(3)		BVS	0.96		mean^2	2.84		mean^2	2.86
				– S7	3.83(2)			*(0.84)*		BVS	3.04		BVS	2.73
	BVS	2.55		mean							*(3.00)*			*(2.90)*
		(2.71)		BVS	1.89									
					(2.16)									
		d (Å)			*d* (Å)			*d* (Å)			*d* (Å)			
Sb5	– S2	2.42(1)	Sb6	– S11	2.44(1)	Sb7	– S4	2.47(5)	Sb8	– S4	2.45(1)			
	– S7	2.52(1)		– S3	2.46(1)		– S13	2.49(9)		– S13	2.61(1)			
	– S7	2.88(2)		– S6	2.78(1)		– S12	2.83(6)		– S12	2.69(2)			
	– S12	2.89(2)		– S11	2.95(1)		– S13	2.93(7)		– S13	3.06(2)			
	– S12	3.18(1)		– S6	3.25(2)		– S12	3.24(9)		– S12	3.12(2)			
	– S13	3.52(1)		– S10	3.57(1)		– S12	3.73(6)		– S12	3.51(1)			
	– S13	3.98(1)					– S12	3.83(7)						
	mean^1	2.68		mean^1	2.66		mean^1	2.68		mean^1	2.58			
	mean^2	2.90		mean^2	2.91		mean^2	2.95		mean^2	2.91			
	BVS	2.74		BVS	2.85		BVS	0.26		BVS	2.33			
		(3.00)			*(3.00)*			*(0.30)*			*(2.70)*			

[1] <Sb–S>, considering Sb–S shorter than 3.0 Å;

[2] <Sb–S>, considering all the Sb–S bonds. BVS: calculated according to the s.o.f. of each S atoms.

* On this basis, for Pb4, among the 13 S ligands, only 9 are present simultaneously.

6.2. Crystallization conditions of disulfodadsonite

As stated above, disulfodadsonite is the Cl-free homeotype of dadsonite, with chlorine being replaced by a disulfide anion $(S_2)^{2-}$; disulfodadsonite is the third well-characterized natural sulfosalt with localized S–S bonding, the others being livingstonite, $HgSb_4S_6(S_2)$, and moëloite, $Pb_6Sb_6S_{14}(S_3)$. Possible additional sulfosalts of the polysulfide type (Moëlo *et al.*, 2008) are museumite, $Pb_2(Pb,Sb)_2S_8(Te,Au)_2$ (Bindi & Cipriani, 2004), and daliranite, $HgPbAs_2S_6$ (Paar *et al.*, 2009), but their crystal structures are still unknown. In addition, a natural diselenide is known, eldragonite, $Cu_6BiSe_4(Se_2)$ (Paar *et al.*, 2012).

The crystallization of these particular mineral phases is linked to high values of $f(S_2)$ in the crystallization medium. According to Craig (1970), livingstonite can only form in geological environments characterized by high values of $f(S_2)$, consistent with its frequent association with native sulfur (Tunell, 1964). Moëloite is the natural counterpart of the 'phase P' synthesized by Moëlo (1983) starting from crushed semseyite with a sulfur excess: also in this case, the critical factor stabilizing moëloite is the very high sulfur

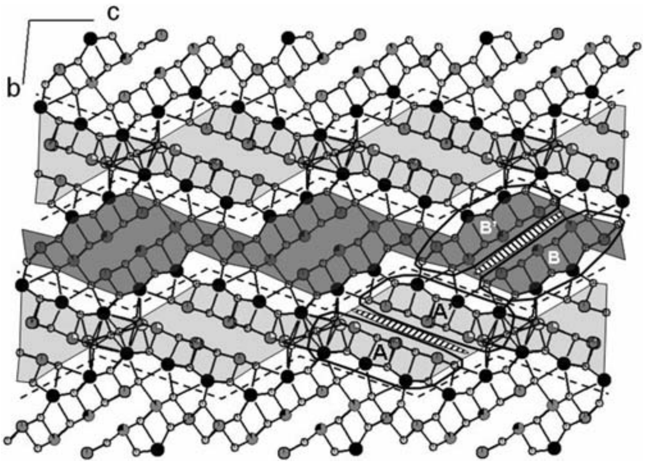

Fig. 3. Projection of the crystal structure of disulfodadsonite along [100]. The **b** axis points downward, and the **c** axis is horizontal. Shading indicates the two kinds of rod-layers, *i.e.* Type-3 rod-layers (dark gray) and Type-5 rod-layers (light gray). In each kind of rod, two sheets, two-atom thick (A/A' and B/B'), are separated by a lone-electron-pair micelle (ruled ellipses).

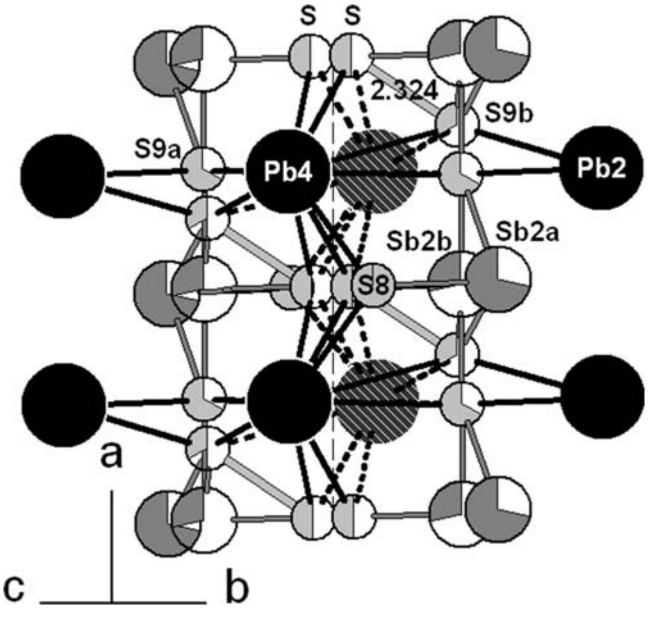

Fig. 4. Environment of unfilled S and (S9a, S9b) positions, and (S–S9b) disulfide anions in the S-rich column connecting the rods in the Type-5 rod-layer of disulfodadsonite.

fugacity. This was confirmed recently by the discovery of a new occurrence of moëloite associated with native sulfur at La Platrière quarry (Wallis, Switzerland; Ansermet *et al.*, 2011). The same conclusion can be hypothesized for disulfodadsonite, which occurs associated with moëloite. At Seravezza, in addition to the two previous sulfosalts, minerals indicating a high sulfur fugacity of the crystallizing medium are native sulfur (relatively frequent), enargite, luzonite, famatinite, colusite, and sulvanite. The association of yellow sphalerite with pyrite is also indicative of a high *f*(S_2) (Scott & Barnes, 1971).

6.3. Comparison with experimental data

Contrary to dadsonite, disulfodadsonite belongs to the pure Pb–Sb–S system. Numerous studies have been devoted to this system, or its sub-set, the PbS–Sb_2S_3 pseudo-binary system. The occurrence of excess S in an unusual oxidation state in disulfodadsonite means that it lies outside that pseudobinary, and must be considered as part of the full Pb–Sb–S ternary system. Secondly, at Ceragiola, the occurrence of robinsonite suggests a relatively high temperature of formation of associated disulfodadsonite, as robinsonite is stable only above 318 °C, according to the experimental data of Craig *et al.* (1973) on the Pb–Sb–S system between 300 and 700 °C. Only sulfosalts on the PbS–Sb_2S_3 pseudo-binary system were found in this first study. Similarly, the study of Garvin (1973) of the Pb–Sb–S system in the same temperature range did not reveal any Pb-Sb sulfosalt with an S-excess. In a more careful study down to 150 °C (Salanci & Klein, 1979; Salanci, 1979), two phases (C and D) were obtained at 270 °C that showed an excess of S. According to Moëlo (1983), the X-ray PDF of phase D corresponds to fülöppite; X-ray data are lacking for phase C. In the study of the Fe–Pb–Sb–S system from 500 °C down to 300 °C, Bortnikov *et al.* (1981) did not observe any sulfosalt with an S excess. Reaction of several Pb-Sb sulfosalts with an S excess at 350 and 375 °C led to moëloite synthesis from semseyite as the starting product, but disulfodadsonite was not detected (Moëlo, 1983).

Due to kinetic constraints, fluid-free synthesis of Pb-Sb sulfosalts at low temperature (below 300 °C) appears very difficult, and published results in this temperature range are incomplete. Disulfodadsonite probably has a narrow stability field, which would explain that experimental studies failed to synthesize it up to now.

6.4. Disulfodadsonite in the framework of Pb/Sb sulfosalt assemblages from Apuan Alps

The hydrothermal systems of the Apuan Alps are a spectacular natural laboratory for the study of the crystal-chemistry of Pb/Sb sulfosalts. Small changes in the physicochemical conditions of the crystallizing medium

Table 7. Comparison between unit-cell parameters of dadsonite (sub-cell, Makovicky *et al.*, 2006) and disulfodadsonite.

	a (Å)	*b*(Å)	*c* (Å)	α (°)	β (°)	γ (°)	*V*(Å^3)	δ*V*(%)
Dadsonite	4.1382	17.394	19.0791	96.442	90.113	90.775	1363.6	
Disulfodadsonite	4.1192	17.4167	19.1664	96.127	90.015	91.229	1366.9	+0.2

could promote the deposition of many different phases. Three main kinds of occurrences can be distinguished: *i*) the Pb-Zn-(Ag) deposits, *ii*) the baryte + pyrite ± iron oxides deposits, and *iii*) the cavities of the Liassic marbles.

The Pb-Zn-(Ag) deposits, hosted in the Paleozoic basement, are well represented by the Bottino mine; they are characterized by a very simple assemblage of Pb/Sb acicular sulfosalts, with boulangerite and meneghinite as the only phases described up to now.

A more complex sulfosalt association has been identified in the second kind of occurrence. These deposits are hosted in a lithologically more complex situation; in fact, sulfosalts have been observed in fractures and veins embedded in lenses of dolostones (Buca della Vena, Monte Arsiccio, and Fornovolasco mines) as well as in the baryte ore (Pollone mine). Very particular $f(O_2)$-$f(S_2)$ conditions and high chlorinity of the hydrothermal solutions (in agreement with the result of several studies on the fluid inclusions, *i.e.* Hodgkins & Stewart, 1994; Lattanzi *et al.*, 1994; Costagliola *et al.*, 1999; Montomoli *et al.*, 2005) were necessary for the crystallization of the rare oxy- and oxy-chloro-sulfosalts firstly described from the Buca della Vena mine, like scainiite (Orlandi *et al.*, 1999), pillaite (Orlandi *et al.*, 2001), pellouxite (Orlandi *et al.*, 2004), and rouxelite (Orlandi *et al.*, 2005). Dadsonite was also described from this occurrence (Orlandi *et al.*, 2010). The Pollone mine belongs to the same kind of deposits (but with some peculiarities, such as the absence of iron oxides). The occurrence of sterryite, closely associated with small grains of famatinite, indicates non-equilibrium conditions relative to the $f(S_2)$ value; indeed sterryite, owing to the presence of localized As–As bonds, points to low $f(S_2)$ conditions, whereas the occurrence of famatinite implies high $f(S_2)$ values (Moëlo *et al.*, 2011, 2012).

The last kind of occurrence of Pb/(Sb-As) sulfosalts is represented by the cavities of the Liassic marbles. The richest locality is the Seravezza marble basin, and this richness can be interpreted as the result of the circulation of hydrothermal fluids generated in the Paleozoic basement, hosting the nearby Bottino Pb-Zn-(Ag) ore deposit. This hypothesis is in agreement with the results of Costagliola *et al.* (1999) on the fluid inclusions in extension veins in the Apuan Alps marble. Seravezza is the type locality of moëloite and disulfodadsonite; as stated above, both minerals are indicative of very high $f(S_2)$. In addition to the type locality, moëloite has been found also in other quarrying districts, such as the Madielle quarries (in the Massa basin), and in the Carrara basin (Orlandi & Criscuolo, 2009).

7. Conclusion

Disulfodadsonite is a new Pb/Sb sulfosalt indicative of a high sulfur fugacity of the crystallization medium, like associated moëloite. At Ceragiola, it was probably formed at relatively high temperature (around 300 °C), but its stability field remains unknown, as experimental studies in the Pb–Sb–S system have not yet permitted to synthesize it.

The mean structure of disulfodadsonite shows its homeotypic derivation from dadsonite. The Cl^- anions of dadsonite are replaced by disulfide anions in disulfodadsonite; these disulfide anions presumably short-range order along the **a** axis, but a superstructure is not formed. In the absence of well-ordered crystals, electron diffraction could be the way to elucidate (S_2) ordering in the S-rich columns at short distance.

The discovery of disulfodadsonite illustrates the complexity and variability of the geochemistry of sulfide ores in the Apuan Alps. Future research in this area may lead to the discovery and characterization of other rare sulfosalts, improving the knowledge of the crystal-chemistry of this mineral group and highlighting the complex history of the hydrothermal systems of this small mountain chain.

Acknowledgements: Electron microprobe analyses were performed with the assistance of O. Rouer (CNRS engineer, Institut des Sciences de la Terre d'Orléans). We are grateful to the mineral collector Francesco Stoppani for providing us with the sample of disulfodadsonite. The manuscript was handled by the Editors Sergey Krivovichev and Luca Bindi. The comments of Andrew G. Christy and Andrew J. Locock helped us in improving the paper.

References

Ansermet, S., Meisser, N., Cuchet, S. (2011): Ein Hauch Carrara im Wallis - zur Mineralogie des Steinbruchs La Plâtrière in Lens. *Schweizer Strahler*, **2/2011**, 2–17.

Bayliss P. (1977): Crystal structure refinement of a weakly anisotropic pyrite. *Am. Mineral.*, **62**, 1168–1172.

Bindi, L. & Cipriani, C. (2004): Museumite, $Pb_5AuSbTe_2S_{12}$, a new mineral from the gold-telluride deposit of Sacarîmb, Metalliferi Mountains, western Romania. *Eur. J. Mineral.*, **16**, 835–838.

Bonaccorsi, E., Merlino, S., Orlandi, P. (2007): Zincalstibite, a new mineral, and cualstibite: crystal chemical and structural relationships. *Am. Mineral.*, **92**, 198–203.

Bortnikov, N.S., Mozgova, N.N., Tsepin, A.I., Breskovska, V.V. (1979): First experiments of synthesis of lead-antimony chloro-sulfosalts. *Dokl. Akad. Nauk SSSR*, **244**, 955–958 (in Russian).

Bortnikov, N.S., Nekrasov, I.Ya., Mozgova, N.N., Tsepin, A.I. (1981): Phases and phase relations in the central portion of the system Fe-Pb-Sb-S between 300 and 500°C in relation to lead-antimony sulphosalts. *N. Jb. Mineral. Abh.*, **143**, 37–60.

Bracci, G., Dalena, D., Orlandi, P., Duchi, G., Vezzalini, G. (1980): Guettardite from Tuscany, Italy: a second occurrence. *Can. Mineral.*, **18**, 13–15.

Brese, N.E. & O'Keeffe, M. (1991): Bond-valence parameters for solids. *Acta Crystallogr.*, **B47**, 192–197.

Bruker AXS Inc (2004): APEX 2. Bruker Advanced X-ray Solutions, Madison, Wisconsin, USA.

Buerger M. (1937): Interatomic distances in marcasite and notes on the bonding in crystals of loellingite, arsenopyrite, and marcasite types. *Z. Kristallogr.*, **97**, 504–513.

Carmignani, L. & Kligfield, R. (1990): Crustal extension in the Northern Apennines: the transition from compression to extension in the Alpi Apuane core complex. *Tectonics*, **9**, 1257–1303.

Costagliola, P., Benvenuti, M., Maineri, C., Lattanzi, P., Ruggieri, G. (1999): Fluid circulation in the Apuane Alps core complex: evidence from extension veins in the Carrara marble. *Mineral. Mag.*, **63**, 111–122.

Craig J.R. (1970): Livingstonite, $HgSb_4S_8$: synthesis and stability. *Am. Mineral.*, **55**, 919–924.

Craig, J.R., Chang, L.L.Y., Lee, W.R. (1973): Investigation in the Pb-Sb-S system. *Can. Mineral.*, **12**, 199–206.

Doussier, C., Moëlo, Y., Meerschaut, A., Léone, P., Guillot-Deudon, C. (2008): Crystal structure of the new compound $Pb_{3+x}Sb_{3-x}S_{7-x}Cl_{1+x}$ ($x \sim 0.45$): the homologous series $Pb_{(2+2N)}(Sb,Pb)_{(2+2N)}S_{(2+2N)}(S,Cl)_{(4+2N)}Cl_N$ and its polychalcogenide derivatives ($N = 1$–3). *J. Solid State Chem.*, **181**, 920–934.

Franceschelli, M. & Memmi, I. (1999): Zoning of chloritoid from kyanite-facies metapsammites, Alpi Apuane, Italy. *Mineral. Mag.*, **63**, 105–110.

Franceschelli, M., Memmi, I., Carcangiu, G., Gianelli, G. (1997): Prograde and retrograde chloritoid zoning in low temperature metamorphism, Alpi Apuane, Italy. *Schweiz. Mineral. Petr. Mitt.*, **77**, 41–50.

Franzini, M., Orlandi, P., Pasero, M. (1992): Morphological, chemical and structural study of robinsonite ($Pb_4Sb_6S_{13}$) from Alpi Apuane, Italy. *Acta Vulcanol.*, Marinelli Volume, **2**, 231–235.

Garvin P.L. (1973): Phase relations in the Pb-Sb-S system. *N. Jb. Mineral. Abh.*, **118**(3), 235–267.

Hodgkins, M.A. & Stewart, K.G. (1994): The use of fluid inclusions to constrain fault zone pressure, temperature and kinematic history – an example from Alpi Apuane, Italy. *J. Struct. Geol.*, **16**, 85–96.

Jolivet, L., Faccenna, C., Goffé, B., Mattei, M., Rossetti, F., Brunet, C., Storti, F., Funiciello, R., Cadet, J.P., d'Agostino, N.., Parra, T. (1998): Midcrustal shear zones in postorogenic extension: example from the northern Tyrrhenian Sea. *J. Geophys. Res.*, **103**, 12123–12160.

Kligfield, R., Hunziker, J., Dallmeyer, R.D., Schamel, S. (1986): Dating of deformational phases using K-Ar and $^{40}Ar/^{39}Ar$ techniques: results from the Northern Apennines. *J. Struct. Geol.*, **8**, 781–798.

Kraus, W. & Nolze, G. (1996): POWDER CELL – a program for the representation and manipulation of crystal structures and calculation of the resulting X-ray powder patterns. *J. Appl. Cryst.*, **29**, 301–303.

Lattanzi, P., Benvenuti, M., Costagliola, P., Tanelli, G. (1994): An overview on recent research on the metallogeny of Tuscany, with special reference to the Apuane Alps. *Mem. Soc. Geol. It.*, **48**, 613–625.

Léone, P., Le Leuch, L.-M., Palvadeau, P., Molinié, P., Moëlo, Y. (2003): Single crystal structures and magnetic properties of two iron or manganese-lead-antimony sulfides: $MPb_4Sb_6S_{14}$ (M: Fe,Mn). *Solid State Sci.*, **5**, 771–776.

Makovicky E. (1993): Rod-based sulphosalt structures derived from the SnS and PbS archetypes. *Eur. J. Mineral.*, **5**, 545–591.

Makovicky, E., Balić-Žunić, T., Karanović, L., Poleti, D., Pršek, J. (2004): Structure refinement of natural robinsonite, $Pb_4Sb_6S_{13}$: cation distribution and modular description. *N.Jb.Mineral.Mh.*, **2004**, 49–67.

Makovicky, E., Topa, D., Mumme, W.G. (2006): The crystal structure of dadsonite. *Can. Mineral.*, **44**, 1499–1512.

Merlino, S. & Orlandi, P. (2001): Carraraite and zaccagnaite, two new minerals from the Carrara marble quarries: their chemical compositions, physical properties, and structural features. *Am. Mineral.*, **86**, 1293–1301.

Molli, G., Giorgetti, G., Meccheri, M. (2000): Structural and petrological constraints on the tectono-metamorphic evolution of the Massa Unit (Alpi Apuane, NW Tuscany, Italy). *Geol. J.*, **35**, 251–264.

Montomoli, C., Ruggieri, G., Carosi, R., Dini, A., Genovesi, M. (2005): Fluid source and pressure-temperature conditions of high-salinity fluids in syn-tectonic veins from the Northeastern Apuan Alps (Northern Apennines, Italy). *Phys. Chem. Earth*, **30**, 1005–1019.

Moëlo Y. (1979): Quaternary compounds in the system Pb-Sb-S-Cl: dadsonite and synthetic phases. *Can. Mineral.*, **17**, 595–600.

— (1983): *Contribution à l'étude des conditions naturelles de formation des sulfures complexes d'antimoine et plomb. Signification métallogénique*. B.R.G.M. ed., Orléans, Document **55**, 624 p.

Moëlo, Y., Makovicky, E., Karup-Møller, S. (1984): New data on the minerals of the andorite series. *N. Jb. Mineral. Mh.*, **1984**, 175–182.

Moëlo, Y., Balitskaya, O., Mozgova, N., Sivtsov, A. (1989): Chlorosulfosels de l'indice plombo-antimonifère des Cougnasses (Hautes-Alpes). *Eur. J. Mineral.*, **1**, 381–390.

Moëlo, Y., Makovicky, E., Mozgova, N.N., Jambor, J.L., Cook, N., Pring, A., Paar, W.H., Nickel, E.H., Graeser, S., Karup-Møller, S., Balić-Žunić, T., Mumme, W.G., Vurro, F., Topa, D., Bindi, L., Bente, K., Shimizu, M. (2008): Sulfosalt systematics: a review. Report of the sulfosalt sub-committee of the IMA commission on ore mineralogy. *Eur. J. Mineral.*, **20**, 7–46.

Moëlo, Y., Orlandi, P., Guillot-Deudon, C., Biagioni, C., Paar, W., Evain, M. (2011): Lead-antimony sulfosalts from Tuscany (Italy). XI. The new mineral species parasterryite, $Ag_4Pb_{20}(Sb_{14.5}As_{9.5})_{\Sigma 24}S_{58}$, and associated sterryite, $Cu(Ag,Cu)_3Pb_{19}(Sb,As)_{\Sigma 22}S_{56}$, from Pollone mine, Tuscany, Italy. *Can. Mineral.*, **49**, 623–638.

Moëlo, Y., Guillot-Deudon, C., Evain, M., Orlandi, P., Biagioni, C. (2012): Comparative modular analysis of two complex sulfosalt structures: sterryite, $Cu(Ag,Cu)_3Pb_{19}(Sb,As)_{22}(As–As)S_{56}$, and parasterryite, $Ag_4Pb_{20}(Sb,As)_{24}S_{58}$. *Acta Crystallogr.*, **B68**, 480–492.

Mumme W.G. (1989): The crystal structure of $Pb_{5.05}(Sb_{3.75}Bi_{0.28})S_{10.72}Se_{0.28}$: boulangerite of near ideal composition. *N.Jb.Mineral.Mh.*, **1989**, 498–512.

Niizeki, N. & Buerger, M.J. (1957): The crystal structure of livingstonite, $HgSb_4S_8$. *Z. Kristallogr.*, **109**, 129–157.

Orlandi, P. (2007): Seit über 2000 Jahren: Marmorabbau in der Toskana. Geologie und Mineralien der Apuaner Alpen. Die Mineralien der Marmorgebiete rund um Carrara, bei Massa und der Versilia. *Lapis*, **7–8/2007**, 15–58.

Orlandi, P. & Criscuolo, A. (2009): *Minerali del marmo delle Alpi Apuane*. Pacini Editore, Pisa, 180 p.

Orlandi, P., Del Chiaro, L., Pagano, R. (1996): Minerals of the Seravezza Marble, Tuscany, Italy. *Mineral. Rec.*, **27**, 47–58.

Orlandi, P., Moëlo, Y., Meerschaut, A., Palvadeau, P. (1999): Lead-antimony sulfosalts from Tuscany (Italy): I – Scainiite,

$Pb_{14}Sb_{30}S_{54}O_5$, the first Pb-Sb oxy-sulfosalt, from Buca della Vena mine. *Eur. J. Mineral.*, **11**, 949–954.

—, —, —, — (2001): Lead-antimony sulfosalts from Tuscany (Italy): III. Pillaite, $Pb_9Sb_{10}S_{23}ClO_{0.5}$, a new Pb-Sb chloro-sulfosalt, from Buca della Vena mine. *Eur. J. Mineral.*, **13**, 605–610.

Orlandi, P., Meerschaut, A., Palvadeau, P., Merlino, S. (2002): Lead-antimony sulfosalts from Tuscany (Italy). V. Definition and crystal structure of moëloite, $Pb_6Sb_6S_{14}(S_3)$, a new mineral from the Ceragiola marble quarry. *Eur. J. Mineral.*, **14**, 599–606.

Orlandi, P., Moëlo, Y., Meerschaut, A., Palvadeau, P., Léone, P. (2004): Lead-antimony sulfosalts from Tuscany (Italy): VI. Pellouxite, ~ $(Cu,Ag)_2Pb_{21}Sb_{23}S_{55}ClO$, a new oxy-chloro-sulfosalt, from Buca della Vena mine. *Eur. J. Mineral.*, **16**, 839–844.

—, —, —, — (2005): Lead-antimony sulfosalts from Tuscany (Italy): VIII. Rouxelite, $Cu_2HgPb_{22}Sb_{28}S_{64}(O,S)_2$, a new sulfosalt from Buca della Vena mine, Apuan Alps: definition and crystal structure. *Can. Mineral.*, **43**, 919–933.

Orlandi, P., Moëlo, Y., Biagioni, C. (2010): Lead-antimony sulfosalts from Tuscany (Italy). X. Dadsonite from the Buca della Vena mine and Bi-rich izoklakeite from the Seravezza marble quarries. *Per. Mineral.*, **79**, 113–121.

Paar, W., Pring, A., Moëlo, Y., Stanley, C.J., Putz, H., Topa, D., Roberts, A.C., Braithwaite, R.S.W. (2009): Daliranite, $PbHgAs_2S_6$, a new sulphosalt from Zarshouran Au-As deposit, Takab region, Iran. *Mineral. Mag.*, **73**, 871–881.

Paar, W., Cooper, M.A., Moëlo, Y., Stanley, C.J., Putz, H., Topa, D., Roberts, A.C., Stirling, J., Raith, J.G., Rowe, R. (2012): Eldragónite, $Cu_6BiSe_4(Se_2)$, a new mineral species from El Dragón mine, Potosí, Bolivia, and its crystal structure. *Can. Mineral.*, **50**, 281–294.

Petrova, I., Kuznetsov, A.I., Belokoneva, E.A., Symonov, M.A., Pobedimskaya, E.A., Belov, N.V. (1978): On the crystal structure of boulangerite. *Dokl. Acad. Nauk SSSR*, **242**, 337–340 (in Russian).

Salanci B. (1979): Beiträge zum System PbS-Sb_2S_3 in Beziehung zu natürlichen Blei-Antimon-Sulfomineralien. *N. Jb. Mineral. Abh.*, **135**(3), 315–326.

Salanci, B. & Klein, D. (1979): Beiträge zum System Pb-Sb-S. *Chem. Erde*, **38**, 105–114.

Scott, S.D. & Barnes, H.L. (1971): Sphalerite geothermometry and geobarometry. *Econ. Geol.*, **66**, 653–669.

Sheldrick G.M. (2008): A short history of SHELX. *Acta Crystallogr.*, **A64**, 112–122.

Skowron, A. & Brown, I.D. (1990): Refinement of the crystal structure of boulangerite, $Pb_5Sb_4S_{11}$. *Acta Crystallogr.*, **C46**, 531–534.

Srikrishnan, T. & Nowacki, W. (1975): A redetermination of the crystal structure of livingstonite, $HgSb_4S_8$. *Z. Kristallogr.*, **141**, 174–192.

Tunell G. (1964): Chemical processes in the formation of mercury ores and ores of mercury and antimony. *Geochim. Cosmochim. Acta*, **28**, 1019–1037.

Wilson, A.J.C., Ed. (1992): International Tables for X-ray Crystallography, Volume C: Mathematical, physical and chemical tables. Kluwer Academic, Dordrecht, NL.

Received 20 February 2013
Modified version received 8 June 2013
Accepted 19 June 2013